

OPEN ACCESS

EDITED BY

Maral Tajerian,
Queens College (CUNY), United States

REVIEWED BY

Giovanni Berardi,
The University of Iowa, United States
Riccardo Collu,
University of Cagliari, Italy
Tiantian Guo,
The University of Chicago, United States

*CORRESPONDENCE

Abhishek Datta
✉ adatta@soterixmedical.com

[†]These authors have contributed equally to this work

RECEIVED 11 November 2024

ACCEPTED 31 March 2025

PUBLISHED 17 April 2025

CITATION

Guillen A, Truong DQ, Cakmak YO, Li S and Datta A (2025) The interplay between pulse width and activation depth in TENS: a computational study.
Front. Pain Res. 6:1526277.
doi: 10.3389/fpain.2025.1526277

COPYRIGHT

© 2025 Guillen, Truong, Cakmak, Li and Datta. This is an open-access article distributed under the terms of the [Creative Commons Attribution License \(CC BY\)](https://creativecommons.org/licenses/by/4.0/). The use, distribution or reproduction in other forums is permitted, provided the original author(s) and the copyright owner(s) are credited and that the original publication in this journal is cited, in accordance with accepted academic practice. No use, distribution or reproduction is permitted which does not comply with these terms.

The interplay between pulse width and activation depth in TENS: a computational study

Alexander Guillen^{1†}, Dennis Q. Truong^{1†}, Yusuf O. Cakmak², Sheng Li³ and Abhishek Datta^{1,4*}

¹Research and Development, Soterix Medical, Woodbridge, NJ, United States, ²Department of Anatomy, University of Otago, Dunedin, New Zealand, ³Department of Physical Medicine and Rehabilitation, McGovern Medical School at The University of Texas Health Science Center at Houston, Houston, TX, United States, ⁴Biomedical Engineering, City College of New York, New York, NY, United States

Background: Transcutaneous electrical nerve stimulation (TENS) has been a commonly used modality to relieve aches and pain for over 40 years. Commercially available devices provide multiple therapy modes involving a different combination of frequency and pulse width with intensity. While frequency sets sensation, intensity helps determine tolerability, longer pulse width is reported to induce a feeling of deeper stimulation. In fact, longer pulse width has been empirically shown to deliver current into deeper tissues, but in context of other electrical stimulation modalities. The goal of this study was to unpack the relationship between pulse width and activation depth in TENS.

Methods: A highly realistic, anatomically-based, 3D finite element model of the forearm was used to simulate the electric field (E-field) distribution, as the pulse width is varied. A typical titration-guided mechanism was used to obtain the strength-duration (S-D) curves of a sensory McIntyre-Richardson-Grill (MRG) axonal model simulating the pain-transmitting A-delta fibers. The pulse widths tested ranged from 30 μ s to 495 μ s.

Results: As expected, shorter pulse widths required more current to achieve activation, resulting in a larger E-field. The S-D curve of the target median nerve indicates a rheobase of 1.75 mA and a chronaxie of 232 μ s. When the applied currents are the same, shorter pulse widths result in a smaller volume of tissue activated (VTA) compared to the longer pulse widths. A 21 fold difference in VTA was found between the longest and shortest pulse widths considered. For the conditions tested in the study, an increase in pulse width resulted in an increase in activation depth, exhibiting a linear relationship.

Conclusion: Our findings highlight the impact of pulse width on activation depth. While choice of a given therapy mode is usually based on an *ad-hoc* desirable sensation basis, medical professionals may consider advocating a certain therapy mode based on the depth of the intended target nerve.

KEYWORDS

transcutaneous electrical nerve stimulation, TENS, chronic pain, simulation, arm model, pulse width, activation depth, penetration depth

1 Introduction

The International Association for the Study of Pain (IASP) defines pain as an unpleasant sensory and emotional experience associated with, or resembling that associated with, actual or potential tissue damage (1). The Centers for Disease Control and Prevention (CDC) estimates that 20.4% (50 million) of American adults suffer

from chronic pain and, of which 8% (19.6 million) live with high-impact chronic pain (2). Chronic pain is further defined by IASP to be pain persisting beyond typical tissue healing time, which is generally considered to be 3 months (3). Common types of chronic pain include back, headache, joint, neck, hip, and osteoarthritis pain (4). Although treatment typically includes pharmacological approaches, one non-pharmacological and non-invasive option recommended by some clinicians for its convenience and effectiveness is Transcutaneous electrical nerve stimulation (TENS) therapy (5).

Studies suggest that TENS helps reduce pain via peripheral and central mechanisms. Conventional TENS activates large diameter afferent fibers which is then sent to the central nervous system to activate descending inhibitory systems to reduce hyperalgesia (6). Specifically, the potential main pathways activated by TENS include projections from the ventrolateral periaqueductal gray (PAG) sending input to the rostroventral medial medulla (RVM), which consequently, projects to the spinal cord to produce analgesia (6, 7). In parallel, studies in fibromyalgia suggest that TENS can restore central pain modulation. Using small battery-powered devices, TENS typically delivers biphasic, symmetric or asymmetric, rectangular or square pulses through cutaneous electrodes positioned near the painful area (6). They can be applied with varying frequencies, from low (<10 Hz) to high (>50 Hz), or mixed frequencies (8). In general, higher-frequency stimulation is delivered at sensory intensity, and low-frequency stimulation is delivered at motor intensity (6). At sensory intensity, patients may experience strong but comfortable sensations without contractions, whereas at high intensity they can feel painless motor contraction (6).

The early evolution of TENS has been characterized by a faster rate of development of clinical applications rather than determining optimal parameters (9). This has been compounded by the fact that use for low back pain was “grandfathered” in the United States. As TENS for low back pain was marketed prior to the 1976 medical device regulation act (10), it was allowed to stay in commerce, and therefore TENS efficacy for low back pain was never “premarket approved”. Newer devices could thereby, obtain marketing “clearance” based on demonstrating equivalence to prior devices based on technology (stimulation parameter) comparison. Given no incentive for device manufacturers to develop proper clinical utility and generate high quality efficacy data, clinical evidence has continued to be debated (4, 5). Newer indications such as TENS for migraine and sinus pain have however demonstrated definitive clinical utility (11–13). TENS devices are considered medium risk (Class 2) devices and are available for both prescription and OTC use.

Commercially available TENS devices for peripheral pain provide multiple therapy modes with each mode delivering a different combination of frequency and pulse width with intensity. The intended use of such devices varies from symptomatic relief of chronic pain associated with sore and aching muscles in the shoulder, waist, back, neck, arm, and leg and/or adjunctive treatment in the management of post-surgical and post-traumatic acute pain. Users are asked to screen through available modes and settle on the mode that provides the “most desirable sensation/comfort”. While frequency selection allows to set desired sensory or

motor contraction, intensity generally maps to tolerability, longer pulse width is suggested to induce a feeling of deeper stimulation.

Studies exploring the effects of pulse width/duration over the years, have mostly studied physiological responses and not the exact relationship to activation depth in TENS. Li and Bak 1976 (14) showed that isolated excitation of different nerve groups (motor, sensory, pain-conducting fibers) in adult cats may be easier with a short duration pulse. Effects on pulse width on the arm have reproduced basic relationships between pulse duration and current intensity found in prior literature (15, 16). Specifically, Alon et al. (9) demonstrated that pain thresholds mediated by pain-conducting fibers in healthy subjects resulted in reducing thresholds (350 mA—30 mA) as pulse duration was increased (5 μ s—1,000 μ s). Further, stimulus pulse width may also be used to selectively recruit fibers of different sizes (17). Some efforts do however come close in context of other electrical stimulation modalities. For instance, increasing pulse width was empirically shown to improve current penetration by reaching distant muscles from surface electrodes in neuromuscular electrical stimulation (NMES) (18). In the context of invasive deep brain stimulation (DBS), increasing pulse width has been shown to lead to activation at greater distances from electrode center (or deeper stimulation) (19, 20). Further, long pulse width stimulation has been shown to penetrate and activate deeper muscles in functional electrical stimulation (FES) (21, 22).

The goal of this computational study was to investigate the effect of the pulse width in TENS on the arm. A high anatomically realistic finite element model was used to simulate the induced electric field (E-field) distribution. The E-field is then coupled to a sensory neuron model given TENS’s efficacy is predicated on providing pain relief by exciting sensory nerves. We evaluated strength-duration (S-D) curve and volume of tissue activated (VTA). The VTA map was related to pulse width to provide insight on the effect of pulse width on activation depth.

2 Methods

2.1 Geometry setup

The computational study was performed using Sim4Life (V7.0.1, Zurich MedTech, Zurich, Switzerland) incorporating NEURON solver (v7.2.3.12730). Sim4Life is a simulation platform that combines human phantoms with relevant physics solvers for analyzing real-world biological problems. Important to this study, the direct integration of the NEURON simulation environment allows seamless application of E-field to neuronal dynamics. The model geometry considered corresponds to the right arm of the Yoon-sun V4-0 dataset (23). The model incorporates high resolution data (0.1 \times 0.1 \times 0.2 mm) making it possible to resolve nerves, arteries, veins, and other small structures. Furthermore, it includes all major nerve trajectories from the cranium and spinal cord to internal organs and muscles and has been used in other peripheral nerve stimulation studies (24, 25). The relevant tissue properties for this study are presented in Table 1 and based on the IT’IS material parameter

TABLE 1 Tissue electrical conductivities (S/m) used in the model.

Tissue	Conductivity	Tissue	Conductivity
Skin	0.1482	Tendon/ ligament	0.3675
Bone (Cancellous)	0.0804	Muscle	0.4610
Bone (Marrow)	0.1797	Air	0
Bone (Cortical)	0.0063	Blood	0.6624
Fat	0.0776	Nerve	0.3475
Subcutaneous adipose tissue (SAT)	0.0776	Gel electrode	1.7

database (26). Precisely, the model in Figure 1A consists of a pair of stimulation electrodes placed at a separation of 2 cm on the wrist with the goal of targeting the median nerve. The electrodes are placed along the length of the median nerve and only serves as a test placement to study the effect of pulse width. The major underlying layers that comprise the model are further indicated in Figures 1B,C. The electrode and interfacing gel combination have a radius of 3 mm with a combined total thickness of 2 mm.

2.2 Nerve trajectories

The intended stimulation region and corresponding nerve anatomy is shown in Figure 2A. While the regions of interest are areas in immediate proximity to the stimulation electrodes, overall visualization of anatomical details in the considered geometry is helpful, to relate to induced E-field and VTA plots. As is known, five specific nerves appear from the cords as the terminal branches of the brachial plexus: musculocutaneous, axillary, radial, median and ulnar nerves. The musculocutaneous nerve provides motor innervation to the muscles of the anterior compartment of the arm (27). The median nerve (comprising C6-T1 spinal roots) predominantly provides motor innervation to the flexor muscles of the forearm and hand (28). The radial nerve innervates most of the skin of the posterior forearm, the lateral dorsum of the hand, and the dorsal surface of the lateral three and a half digits. Lastly, the ulnar nerve carries both sensory and motor fibers and supplies sensory cutaneous innervation to the medial forearm, medial wrist, and medial one and one-half digits (27).

The longest trajectories of the ventral and dorsal roots of C6 and T1 were considered for analysis here (Figure 2B) due to the expected direct influence on the mid-forearm—based on electrode locations. The nerve depth from skin in contact with electrodes to the median nerve is about 5.5 mm, the radial nerve is about 13.1 mm, and the ulnar nerve is 14.9 mm. The three “point sensor” locations along the nerve trajectory used for collecting the simulation data (i.e., nodes 520, 550, and 580) are illustrated in Figure 2C. There were therefore 18 point sensors considered: 9 (ventral rami) and 9 (dorsal rami).

2.3 Injected current

The low-frequency electromagnetic (EM LF)—Ohmic Quasi-Static module, a rectilinear LF solver, was used to simulate TENS

on the arm at multiple pulse widths (30, 88, 146, 262, and 495 μ s) corresponding to the range typically available in commercial TENS stimulators. Specifically, the goal was to simulate the impact of a single pulse. Dirichlet boundary conditions were applied as 2.38 V and -2.38 V at the anode and cathode corresponding to 5 mA of current flux calculated on the electrodes. Other external boundaries were electrically insulated (i.e., normal current density = 0). The Ohmic quasi-static field as noted in Equation 2.1

$$\nabla \cdot \sigma \nabla \phi = 0 \quad (2.1)$$

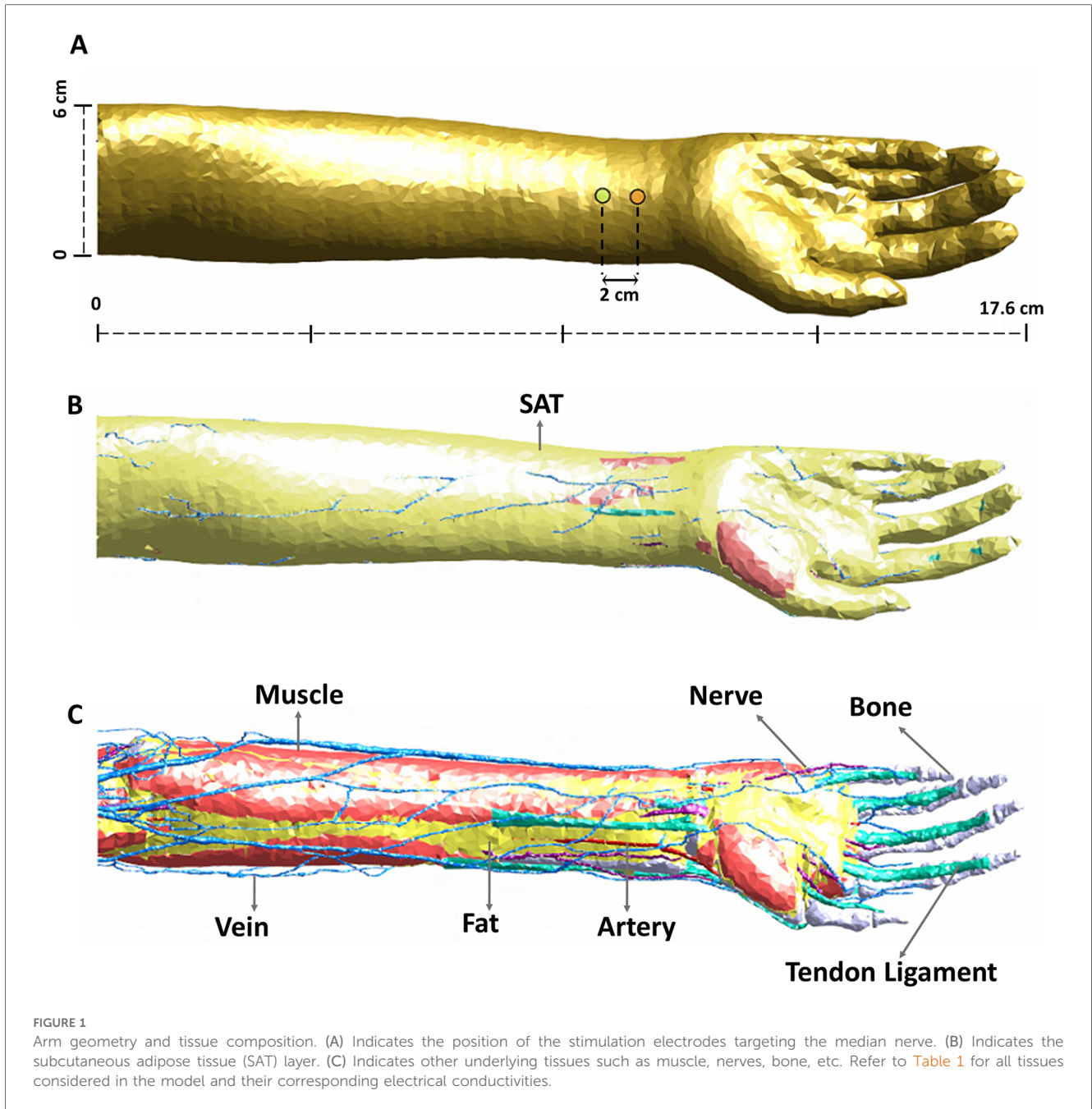
was solved with the aforementioned boundary conditions for the electric potential distribution (29–31). The injected current was then re-calculated based on the titration factor (see section on Titration mechanism) to visualize differences in the E-field between the different pulse widths.

2.4 Neuron model and additional simulation considerations

TENS is known to stimulate sensory nerves, suppressing the pain signals being sent to the brain to give user relief. We therefore considered the sensory McIntyre-Richardson-Grill (MRG) neuron model (32, 33), with the smallest diameter setting available (5 μ m), to simulate the effects of pain-transmitting nerve fibers. The MRG model is based on a double-cable representation of the axon that allows separating electrical representations of the myelin and underlying internodal axolemma. The model has been used for neural predictions in a variety of applications (20, 34, 35). Specific to this study, a modified MRG model that considers electrophysiological properties of sensory fibers was considered (34). For simulating TENS using the titration mechanism, the modulation pulse type was set to bipolar with a unitless amplitude of 1 and an interphase interval of 0.1 ms while varying the pulse widths. Therefore, each of the five pulse widths considered, were individually simulated. The duration and time step of the solver were set to 3.5 ms and 0.0025 ms respectively. The junction potential was not corrected. Running a simulation for the aforementioned nodes of interest at one pulse width took approximately 4 h using 64 threads on a workstation with the following specifications: AMD Ryzen Threadripper 3970X 32-Core Processor, 3.70 GHz CPU speed, and 192 GB installed RAM.

2.5 Titration mechanism

Titration involves stimulating an axon with a series of modulating pulses of *increasing* intensity to find the threshold at which a single action potential is generated in excitable cells. This method introduces an additional scaling factor that is titrated until a response can be detected within the stimulated



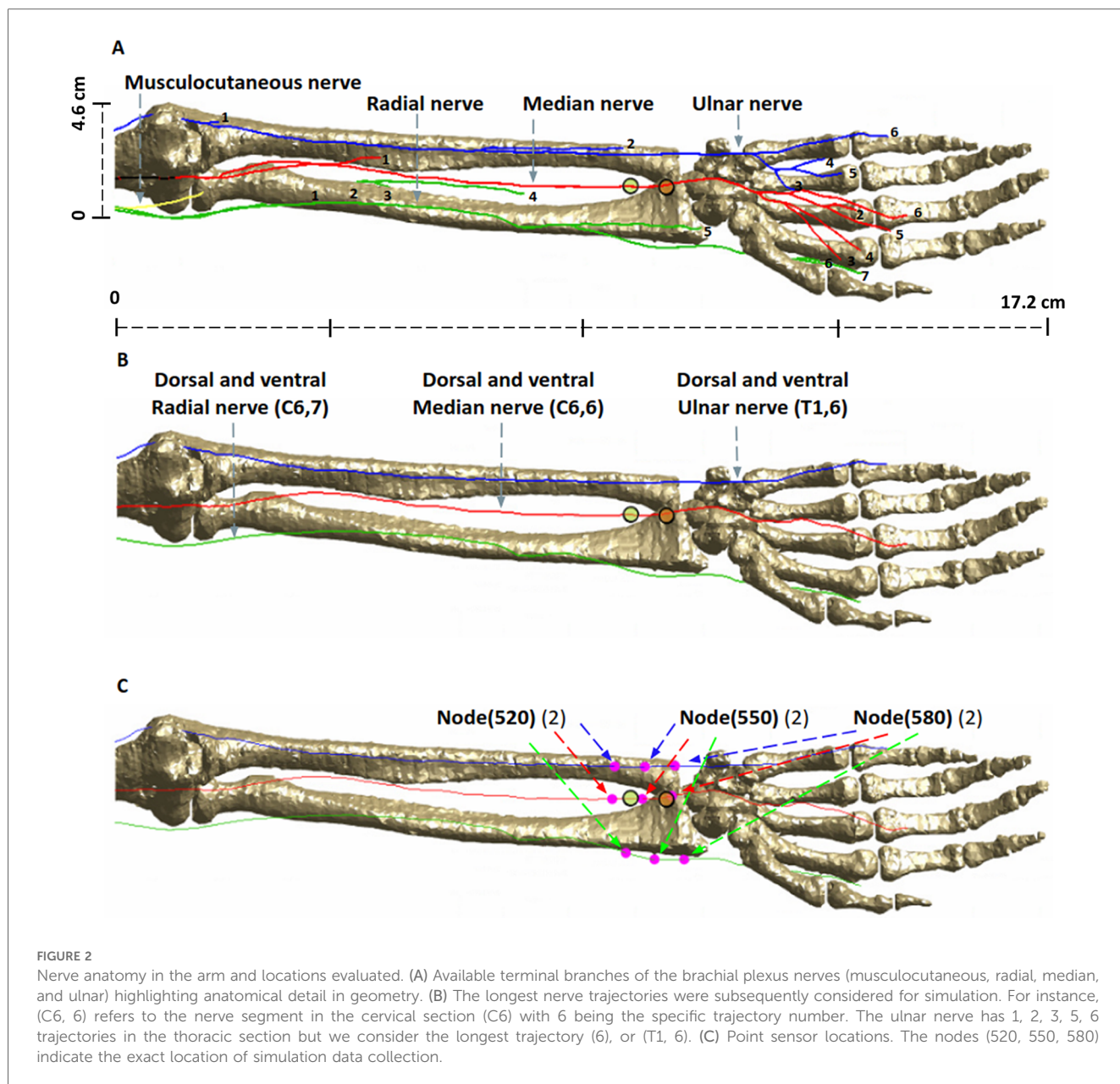
region (36, 37). Thus, the excitability threshold (I_T) as indicated in Equation 2.2 is the product of the current applied to the cellular membrane of the axon, the aforementioned titration factor (T), and the modulating pulse ($a(t)$):

$$I_T(t) = I.T.a(t) \tag{2.2}$$

The T parameter is considered as a scaling factor to indicate proportion or a multiple of the actual modulated current needed to generate an action potential. Potential and current can be used interchangeably here for measuring the stimulus strength.

2.6 Volume of tissue activated

The volume of tissue activated (VTA) was used to compare stimulation differences caused by changes in pulse width. The VTA around each electrode contact relied on the concept of activation function (AF), which was calculated from the eigenvalues of the Hessian matrix (38). Each eigenvalue of the Hessian matrix represents the second partial derivative of the electric potential along the respective eigenvector. A multi-step process was used to determine the VTA due to pulse width variation. This involved determining the excitability threshold (I_T), using the corresponding electric potential to calculate the AF, and subsequently utilizing the AF to determine the VTA.



3 Results

3.1 Electric field (E-field)

The induced *surface* E-field plots due to the shortest and the longest pulse widths, calculated at their corresponding titration factors (see Table 2) and plotted to the same scale, are included in Figure 3. As mentioned above, these simulations reflect the impact of a single pulse. The plots reveal that the smaller pulse width (30 μs) induces a larger E-field (max: 456 V/m)—covering a larger area of the arm. On the other hand, the induced E-field due to 495 μs is less diffuse, more focused, and has lower magnitude from the same pair of electrodes. However, this is intuitively expected, as the plots are generated at their respective stimulation threshold, so the 30 μs E-field is the result of 19.7 mA and the

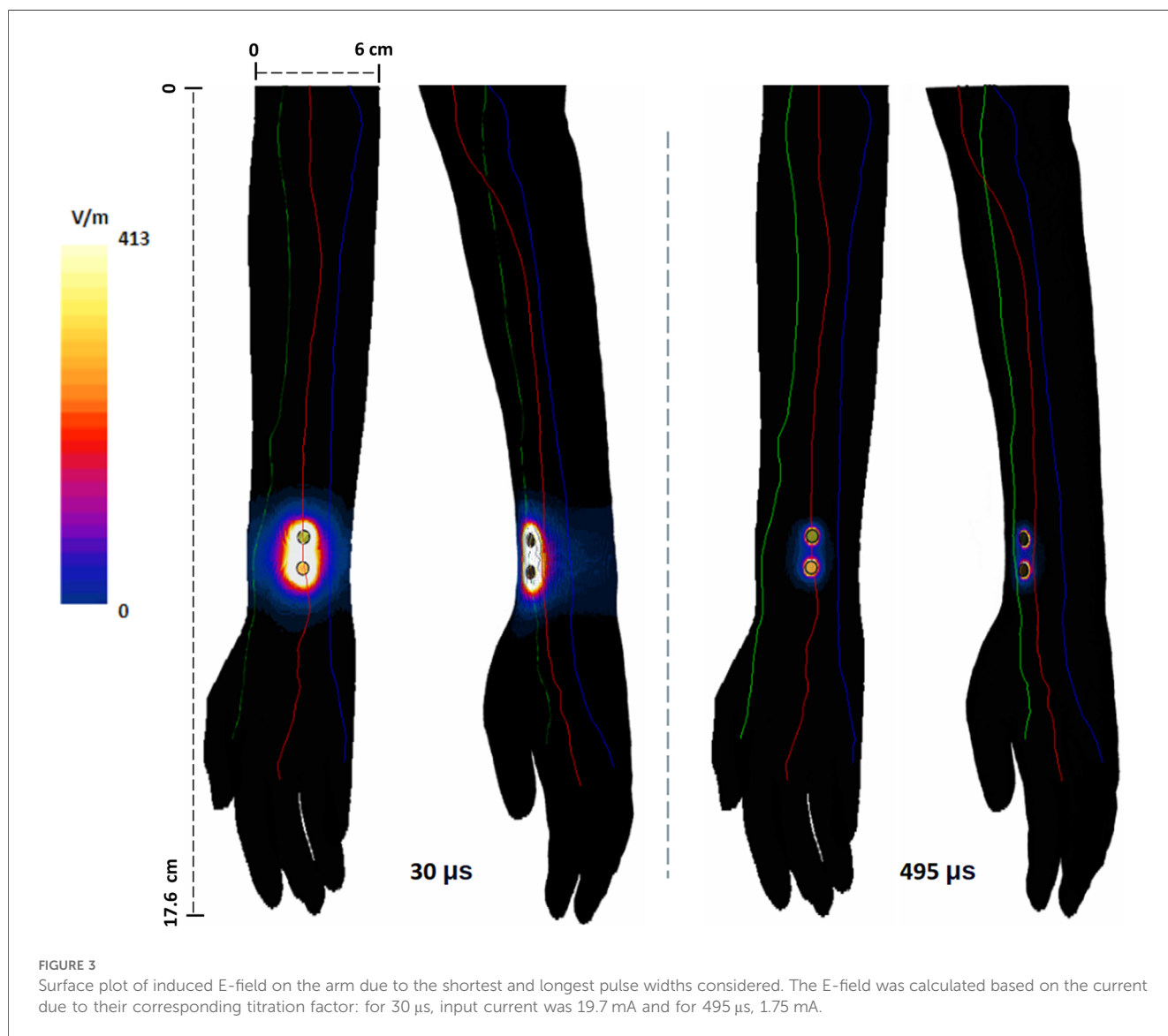
495 μs E-field is the result of injecting 1.75 mA. The overall spatial profile resembles a stretched ellipse with the major axis along the line connecting the stimulation electrodes. The ulnar and radial nerves that are farther away from the electrode sites receive less E-field (~0 to 132 V/m). With longer pulse width, the induced E-field profile in the immediate vicinity of the electrode sites indicates a restricted hot-spot with dramatic fall-off (~40 to 280 V/m) and approximately 0–23 V/m for the rest of the nerves.

3.2 Titration factor

As previously stated, the titration technique was employed to find the threshold potential of membrane depolarization. Table 2 notes the individual titration factors and the corresponding

TABLE 2 Titration factor and corresponding excitability threshold current at chosen sensor locations. Values are noted for the shortest (30 μ s) and longest (495 μ s) pulse duration at sensor nodes (520, 550, 580). As expected, minimum titration factors and current were needed for the superficial median nerve with the highest values needed for the ulnar nerve.

C6 dorsal		C6 ventral		T1 dorsal		T1 ventral	
Median (30 μ s)	3.93 (19.65 mA)	Median (30 μ s)	3.93 (19.65 mA)	Ulnar (30 μ s)	81.55 (407.75 mA)	Ulnar (30 μ s)	76.57 (382.85 mA)
Median (495 μ s)	0.34 (1.7 mA)	Median (495 μ s)	0.34 (1.7 mA)	Ulnar (495 μ s)	11.31 (56.55 mA)	Ulnar (495 μ s)	10.87 (54.35 mA)
Radial (30 μ s)	35.57 (177.85 mA)	Radial (30 μ s)	35.57 (177.85 mA)				
Radial (495 μ s)	3.21 (16.05 mA)	Radial (495 μ s)	3.21 (16.05 mA)				



excitability threshold current needed for the roots (C6 and T1). As expected, the titration factor is substantially smaller for the 495 μ s pulse in comparison to the 30 μ s pulse. While the titration factors of dorsal and ventral sections for the C6 roots are the same, they differ somewhat for the T1 roots. Further, as anticipated, minimum titration factors and current were needed in the branches of the median nerve due to the proximity to the electrode sites.

3.3 Strength-duration curve

The resulting strength-duration (S-D) curve of the median nerve under electrical stimulation is shown in [Figure 4](#). For the range of 30–495 μ s considered here, the rheobase was found to be \sim 1.75 mA with a chronaxie of \sim 232 μ s. Consistent with the theory, the curve tends to flatten out with longer stimulus duration (or pulse width).

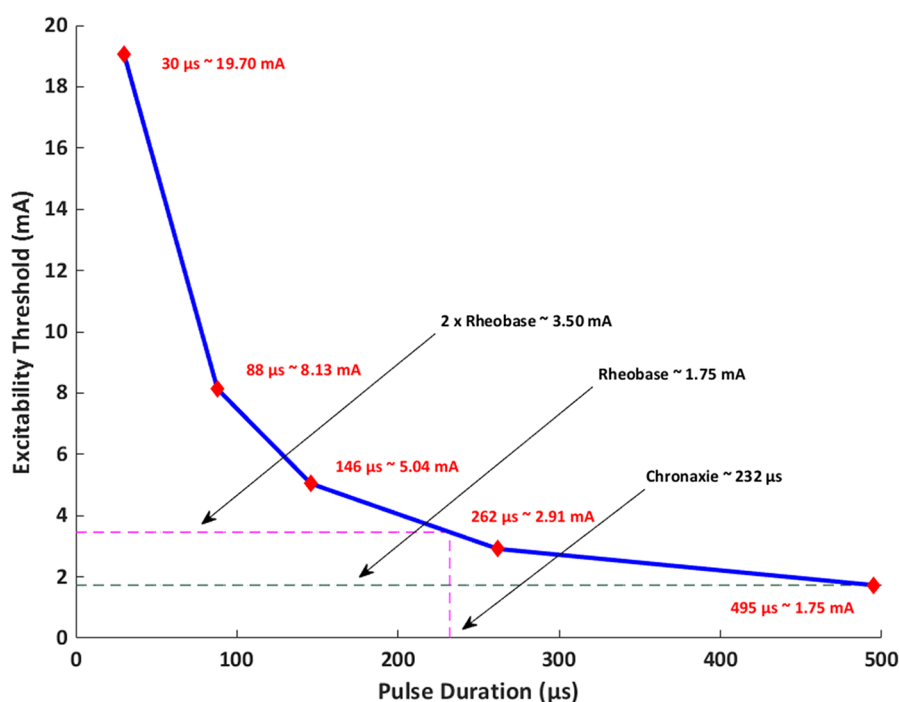


FIGURE 4

Strength-duration (S-D) curve of the target median nerve. A pulse width range of 30–495 µs was considered in the study. The corresponding excitability threshold for each pulse width is noted along the curve.

3.4 Volume of tissue activated (VTA)

The VTA maps illustrate isosurface plots derived from the absolute value of Hessian matrix eigenvalues of the electric potential. Since the Hessian matrix is essentially a matrix of the second partial derivative of the electric potential, it enables determination of the classic activating function in 3D (39, 40). To facilitate a direct comparison across the range of pulse widths considered, we plotted the VTA maps at one common current value- i.e., the average threshold current (10.73 mA) spanning the shortest and longest pulse widths (Figure 5). As expected, the shortest pulse width requires the highest threshold to activate tissue near the input source and is approximately a factor of 11 higher with respect to the longest pulse width ($8.8 \text{ e}^5/7.82 \text{ e}^4$). The estimated VTA for the shortest and widest pulses were 118.72 mm^3 and $2,586.24 \text{ mm}^3$ respectively, indicating a VTA ratio of 21.2.

The value of this study is exemplified by observing the shape and pattern of the VTA maps. While VTA investigation in invasive applications such as DBS reveal uniform “blobs” around the electrode contacts reflecting *one* brain region (19, 41), the maps here are scattered and irregular, due to varying complex anatomy. This is only captured due to the realistic arm geometry considered here. The VTA maps also help visualize the influence of pulse width on activation depth. The plots in the first column indicate that for pulse widths up to 146 µs, it is not possible to recruit the deeper radial and the ulnar nerves. At the longest pulse width, there is some activation at the levels of the deeper nerves of the arm.

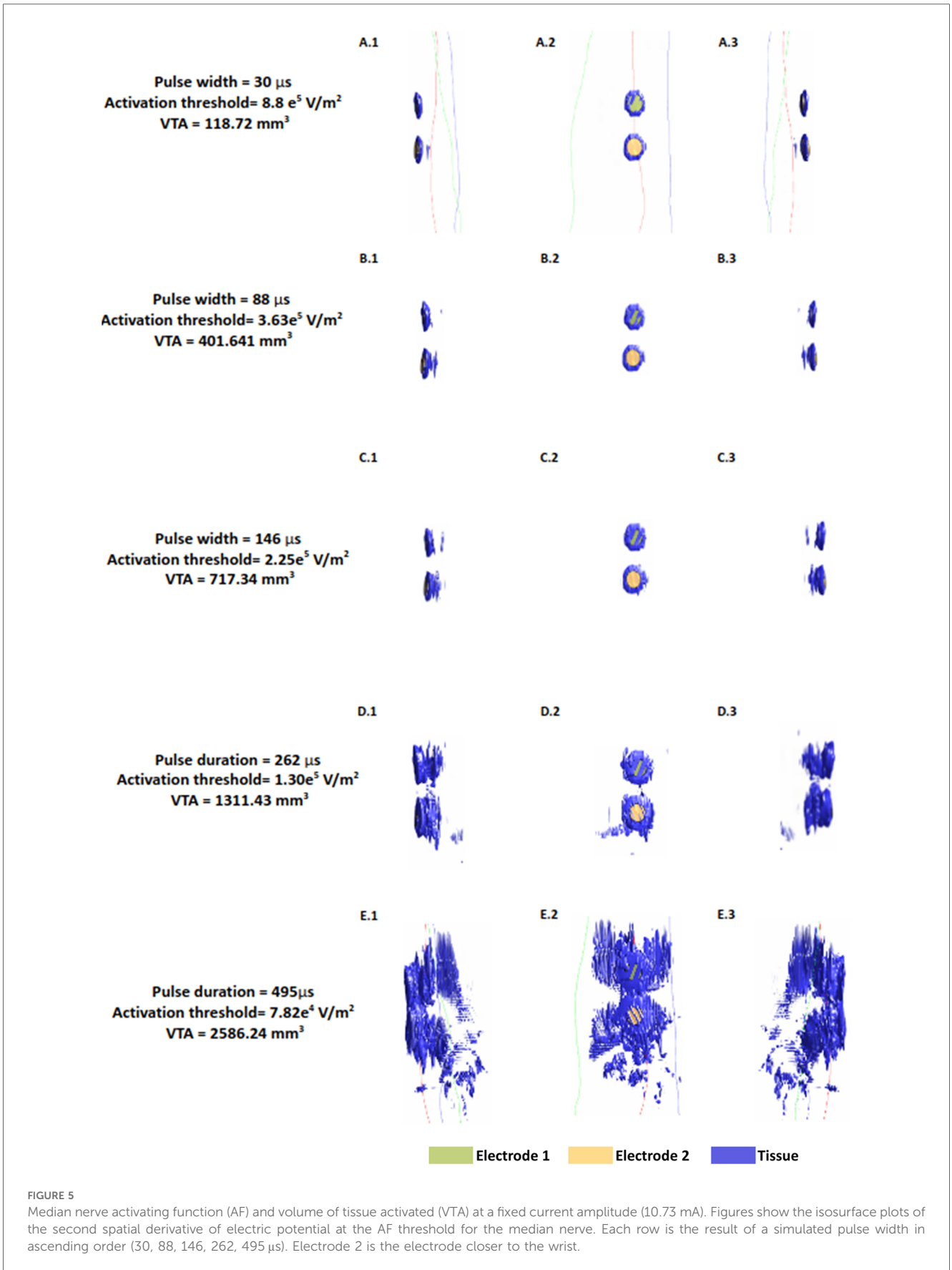
3.5 Influence of the pulse width with respect to activation depth

To understand the influence of pulse width on activation depth, we plotted predicted VTA with respect to the varying pulse widths considered (Figure 6). We note a linear relationship for the range of pulse widths considered here.

4 Discussion

The central aim of this study was to unpack the relationship between pulse width and activation depth during TENS on the arm. Prior electrical stimulation studies using other modalities have empirically shown that wider pulses can recruit deeper targets. Using a highly detailed 3D model, we provide enhanced visualization of available geometry, induced E-field profile, VTA maps, and relationship to activation depth, for the first time.

The S-D curves for nerve stimulation have clearly established its shape over numerous investigations dating back to the 30's (42–45). Given the dominant electrical capacitance of the neural membrane, S-D curves expectedly follow a capacitor discharge curve. A TENS practitioner can therefore readily use the inverse relationship between intensity and pulse width to make an informed stimulation strategy choice. Now longer pulse widths at the same current would lead to more charge delivered across the membrane- presumably translating to deeper stimulation. However, the exact relationship has not been explored previously



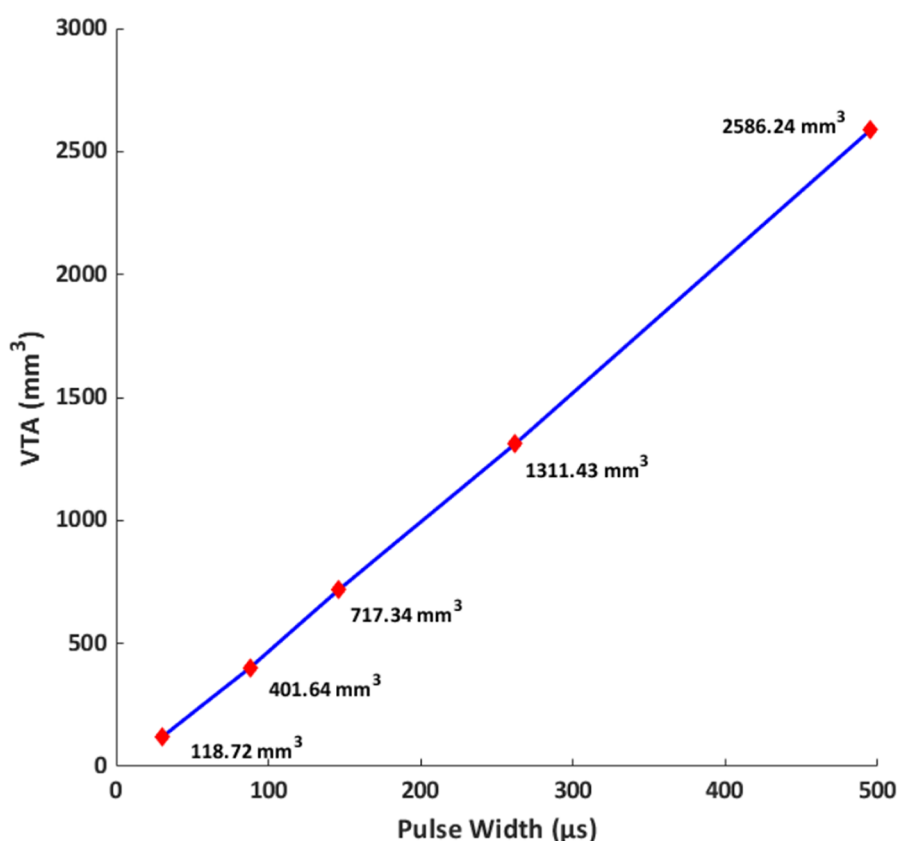


FIGURE 6

Volume of tissue activated (VTA) vs. pulse width at a fixed current amplitude (10.73 mA). VTA is used as a surrogate for activation depth. For the range of pulse widths and conditions considered here, the relationship is linear.

in TENS. Further for non-invasive electrical nerve stimulation applications, lowering pulse width in order to deliver higher current intensity is limited to the intensity at which the user can comfortably receive stimulation (46). This restriction is however not applicable for invasive delivery (20) as stimulation does not have to navigate superficial cutaneous sensation.

The linear relationship between VTA and pulse width observed in our simulations indicates that longer widths would lead to deeper activation. We note that our observations are restricted to only the pulse widths and the concomitant geometry (forearm) considered here. We expected the relationship to asymptote at higher pulse widths as the excitability threshold reaches rheobase. While the excitability threshold in the S-D curve (Figure 4) follows a hyperbolic or exponential decay similar to classical equations [Weiss-Lapique and Lapique-Blair (44, 45)], the VTA expands with a similar convexity resulting in a *net* linear VTA—pulse width relationship. We suspect this is due to (1) volume being cubic and (2) the Hessian of voltage dropping exponentially away from the electrodes. There are several limiting assumptions to the plot. We are considering only the magnitude of the Hessian, which does not account for orientation/alignment with any possible axon. The AF thresholds were calibrated for the median nerve A-delta fiber running along the length of the arm; other nerve orientations and fiber types would be expected

to respond differently. Further, heterogeneous tissues cause spikes in E-field and AF at material boundaries. Additionally, the MRG model is a simplification of real nerves (i.e., devoid of complex morpho-electric properties) and does not incorporate all ion channel sub-types. It is therefore possible that the lack of model complexity masks non-linearities.

TENS efficacy is likely predicated upon a net effect of stimulating multiple underlying nerves of various types including discharge frequencies. We note that we simply used the median nerve in this study as a test nerve to explore relationships between E-field, strength, duration, activation depth, etc. However, the choice of A-delta fiber is rational as nociceptors generally transmit noxious stimuli through A-delta and C-fiber nerves (47). Further, it is known that the C-fiber afferents carry slow sensations associated with aches, whereas the A-delta afferents are associated with fast sensations such as sharp pain. Given the type of pain felt and if one were to know underlying nerve depth (47), one could potentially start with a suitable pulse width. In reality however, pre-programmed therapy modes (combination of pre-set frequency and pulse width) are provided in TENS devices for pain relief, limiting full flexibility to the user in parameter selection. Therefore, the best approach continues to be to try all modes first, and in each case, titrating intensity to the strongest possible but at a level that is comfortable. If deeper

pain relief is desired, patients may consider picking the next mode with longer pulse width while maintaining the frequency and intensity from the prior mode. The caveat however, is that overall pain relief is contingent not only on pulse width parameter of TENS but other factors including discharge frequency, temporal and spatial summation of signals, segmental and central pain mechanisms should also be accounted.

The strength of our modeling process in simulating TENS on the arm is the usage of a highly realistic model. Previous 3-D FEM approaches have either used *idealized* geometries such as a cylindrical arm (48–50) or derived from 2-D anatomical images by extruding geometry (37) and limiting to certain cross sections (34). The modeling methodology applied here, from the geometry, applying EM simulations into a dynamic Neuron solver, using the modified MRG model, and subsequently using titration analysis, mimics the one employed in the context of magnetic stimulation (MS) (24). The simulation setup used in the aforementioned MS study has been further validated using clinical experiments. Specifically, numerically estimated latencies and waveforms were in agreement with the empirical measurements on subjects undergoing MS on the arm (25). The only difference to our simulation is the application of electrical stimulation and thereby, related governing equation. However, the governing equation is a standard equation used to predict induced current in volumetric media and has been validated in other applications (51, 52). Further, the MRG model has been shown to generate accurate predictions for TENS specifically, compared to active cable and mammalian nerve models (29, 37). Taken together, we expect the main conclusions of this study to be robust.

We specifically isolated the effects due to pulse width given the main aim of our study. In reality, pulse widths are associated with pulse repetition frequency and it is well known that frequency also allows for selective nerve activation. However, this isolation was needed to unpack the relationship of pulse width to activation depth.

It is further meaningful to compare our simulation results to previous experimental attempts. When Kuhn et al., (48) tested three volunteers using 5 × 5 cm electrodes placed on Flexor Digitorum Superficialis and on the wrist, the S-D curve at 0.5 ms indicated a corresponding intensity of ~5 mA. Goffredo and colleagues tested direct stimulation of the median nerve at the biceps brachii level using a pair of round electrodes (1.5 cm diameter) on six subjects (49). The S-D curve based on experiments indicated intensities of ~16 mA and ~9 mA at pulse widths of 200 μs and 500 μs respectively. When considering smaller diameter A-beta fibers to study tactile sensation and 9 mm diameter electrodes on forearm (separation = 12 mm) on six subjects, S-D curve indicated a ~1.7 mA multiples of rheobase at 200 μs pulse width (50). Finally, Gaines and colleagues report good agreement with historical experimental data with multiples of rheobase of ~6 V and a chronaxie of 230 μs for a sensory axon (10 μm diameter) (34). The region of interest was the arm near the elbow. We note that a one-to-one comparison across aforementioned efforts and our simulations is non-trivial due to several differences—from geometry (3D

forearm is different to 3D upper arm), specific stimulation electrode montage (size and separation)/induced E-field distribution, nerve fiber/related properties considered, etc. Notwithstanding, our predictions of 1.75 mA (rheobase) and 232 μs (chronaxie) considering the median nerve in the forearm are in the range of experimentally shown values. For similar reasons, extrapolating our predictions to other body parts is not possible due to geometrical, electrode placement, and nerve fiber differences.

There are practical limitations to increasing the pulse width at the same current intensity to increase activation depth, namely battery life. The chronaxie is usually considered the most efficient pulse width choice for conserving the pulse generator's battery life and is naturally a key factor in invasive applications (53). With modern day TENS devices powered by high capacity small rechargeable batteries, this is not much of a concern. However, as mentioned above, we expect the linear relationship to ultimately change and plateau. Promising solutions such as coupling TENS with a nerve cuff to facilitate activation of deeper nerves has been proposed (37). However, nerve cuff involves surgery and moreover, such solutions are still being developed and not currently available to the practitioner or the patient.

Computational modeling and simulation such as the one reported here is now increasingly used across a range of stimulation modalities, from optimizing delivery, performing safety analysis, to supporting device design/development (31, 41, 54–57). Furthermore, these predictions have helped in elucidating stimulation parameter choices, understanding mechanism of action, explaining stimulation outcome, and thereby advancing stimulation administration in general (13, 58–62). We expect this study on the arm to guide researchers in performing future explorations on other body parts, determine ideal pulse width range for target nerve of interest, attempt validation using TENS like the one performed in MS (25), and investigate new TENS delivery approaches (63). One could screen across different electrode montages (i.e., electrode separation, size, and shape) to optimally deliver stimulation to a desired target. Modalities such as interferential (IF)/temporal interference stimulation is now being studied in brain using high resolution anatomical models (64), but it has existed in peripheral stimulation since the 50s (65). Our simulations could be further expanded to study IF stimulation for specific peripheral targets.

5 Conclusions

Stimulation parameter selection during TENS programming for pain relief is typically based on an ad-hoc sensation basis. Using a highly detailed and realistic 3D arm model, we demonstrate a linear relationship between commonly available pulse width settings and activation depth for TENS on the forearm. While multiple factors impact overall pain relief, once frequency and intensity are set, medical professionals may consider choosing a certain pulse width setting based on the depth of pain relief desired. One can expect a 21 fold difference

in volume of tissue activated across the range of pulse width settings available in commercially available devices.

Data availability statement

The original contributions presented in the study are included in the article/Supplementary Material, further inquiries can be directed to the corresponding author.

Author contributions

AG: Data curation, Formal analysis, Investigation, Methodology, Software, Validation, Visualization, Writing – original draft, Writing – review & editing. DT: Data curation, Formal analysis, Investigation, Methodology, Software, Supervision, Validation, Visualization, Writing – review & editing. YC: Supervision, Validation, Writing – review & editing. SL: Supervision, Validation, Writing – review & editing. AD: Conceptualization, Formal analysis, Funding acquisition, Investigation, Methodology, Project administration, Resources, Software, Supervision, Validation, Visualization, Writing – original draft, Writing – review & editing.

Funding

The author(s) declare that financial support was received for the research and/or publication of this article. AD is supported by grants from the National Institute of Health (NIH): 75N95020C00024, Department of Defense (DOD): W81XWH22C0111, and National Aeronautics and Space Administration (NASA): 80NSSC22CA071.

References

- Raja SN, Carr DB, Cohen M, Finnerup NB, Flor H, Gibson S, et al. The revised international association for the study of pain definition of pain: concepts, challenges, and compromises. *Pain*. (2020) 161(9):1976–82. doi: 10.1097/j.pain.0000000000001939
- Dahlhamer J, Lucas J, Zelaya C, Nahin R, Mackey S, DeBar L, et al. Prevalence of chronic pain and high-impact chronic pain among adults—United States, 2016. *MMWR Morb Mortal Wkly Rep*. (2018) 67(36):1001–6. doi: 10.15585/mmwr.mm6736a2
- Treede RD, Rief W, Barke A, Aziz Q, Bennett MI, Benoliel R, et al. Chronic pain as a symptom or a disease: the IASP classification of chronic pain for the international classification of diseases (ICD-11). *Pain*. (2019) 160(1):19–27. doi: 10.1097/j.pain.0000000000001384
- Cohen SP, Vase L, Hooten WM. Chronic pain: an update on burden, best practices, and new advances. *Lancet*. (2021) 397(10289):2082–97. doi: 10.1016/S0140-6736(21)00393-7
- Johnson MI, Paley CA, Jones G, Mulvey MR, Wittkopf PG. Efficacy and safety of transcutaneous electrical nerve stimulation (TENS) for acute and chronic pain in adults: a systematic review and meta-analysis of 381 studies (the meta-tens study). *BMJ Open*. (2022) 12(2):e051073. doi: 10.1136/bmjopen-2021-051073
- Vance CG, Dailey DL, Rakel BA, Sluka KA. Using TENS for pain control: the state of the evidence. *Pain Manag*. (2014) 4(3):197–209. doi: 10.2217/pmt.14.13
- DeSantana JM, Walsh DM, Vance C, Rakel BA, Sluka KA. Effectiveness of transcutaneous electrical nerve stimulation for treatment of hyperalgesia and pain. *Curr Rheumatol Rep*. (2008) 10(6):492–9. doi: 10.1007/s11926-008-0080-z

Acknowledgments

This research was sponsored by the Department of Defense (DOD) under contract # W81XWH22C0111 awarded to Soterix Medical, Inc. The opinions expressed herein are those of the authors and do not reflect those of the United States government. The U.S. government is authorized to reproduce and distribute reprints for Government purposes notwithstanding any copyright notation herein.

Conflict of interest

AG, DT, and AD are employees of Soterix Medical, Inc.

The remaining authors declare that the research was conducted in the absence of any commercial or financial relationships that could be construed as a potential conflict of interest.

Generative AI statement

The author(s) declare that no Generative AI was used in the creation of this manuscript.

Publisher's note

All claims expressed in this article are solely those of the authors and do not necessarily represent those of their affiliated organizations, or those of the publisher, the editors and the reviewers. Any product that may be evaluated in this article, or claim that may be made by its manufacturer, is not guaranteed or endorsed by the publisher.

- Vance CG, Dailey DL, Chimenti RL, Van Gorp BJ, Crofford LJ, Sluka KA. Using tens for pain control: update on the state of the evidence. *Medicina (B Aires)*. (2022) 58(10):1332. doi: 10.3390/medicina58101332
- Alon G, Allin J, Inbar GF. Optimization of pulse duration and pulse charge during transcutaneous electrical nerve stimulation. *Aust J Physiother*. (1983) 29(6):195–201. doi: 10.1016/S0004-9514(14)60670-X
- Aboy M, Crespo C, Stern A. Beyond the 510(k): the regulation of novel moderate-risk medical devices, intellectual property considerations, and innovation incentives in the FDA's de novo pathway. *NPJ Digit. Med*. (2024) 7:29. doi: 10.1038/s41746-024-01021-y
- Riederer F, Penning S, Schoenen J. Transcutaneous supraorbital nerve stimulation (T-SNS) with the Cefaly® device for migraine prevention: a review of the available data. *Pain Ther*. (2015) 4:135–47. doi: 10.1007/s40122-015-0039-5
- Goldsobel AB, Prabhakar N, Gurfein BT. Prospective trial examining safety and efficacy of microcurrent stimulation for the treatment of sinus pain and congestion. *Bioelectron Med*. (2019) 5:18. doi: 10.1186/s42234-019-0035-x
- Thomas C, Truong DQ, Lee K, Deblieck C, Androurakis XM, Datta A. Determination of current flow induced by transcutaneous electrical nerve stimulation for the treatment of migraine: potential for optimization. *Front Pain Res (Lausanne)*. (2021) 2:753454. doi: 10.3389/fpain.2021.753454
- Li CL, Bak A. Excitability characteristics of the A- and C-fibers in a peripheral nerve. *Exp Neurol*. (1976) 50(1):67–79. doi: 10.1016/0014-4886(76)90236-3
- Crago PE, Peckham PH, Mortimer JT, Van der Meulen JP. The choice of pulse duration for chronic electrical stimulation via surface, nerve, and

- intramuscular electrodes. *Ann Biomed Eng.* (1974) 2(3):252–64. doi: 10.1007/BF02368496
16. Moreno-Aranda J, Seireg A. Electrical parameters for over-the-skin muscle stimulation. *J Biomech.* (1981) 14(9):579–85. doi: 10.1016/0021-9290(81)90083-X
17. Szlavik RB, de Bruin H. The effect of stimulus current pulse width on nerve fiber size recruitment patterns. *Med Eng Phys.* (1999) 21(6–7):507–15. doi: 10.1016/S1350-4533(99)00074-0
18. Doucet BM, Lam A, Griffin L. Neuromuscular electrical stimulation for skeletal muscle function. *Yale J Biol Med.* (2012) 85(2):201–15.
19. Astrom M, Diczfalusy E, Martens H, Wardell K. Relationship between neural activation and electric field distribution during deep brain stimulation. *IEEE Trans Biomed Eng.* (2015) 62(2):664–72. doi: 10.1109/TBME.2014.2363494
20. Anderson CJ, Anderson DN, Pulst SM, Butson CR, Dorval AD. Neural selectivity, efficiency, and dose equivalence in deep brain stimulation through pulse width tuning and segmented electrodes. *Brain Stimul.* (2020) 13(4):1040–50. doi: 10.1016/j.brs.2020.03.017
21. Kern H, Carraro U. Home-based functional electrical stimulation of human permanent denervated muscles: a narrative review on diagnostics, managements, results and byproducts revisited 2020. *Diagnostics (Basel).* (2020) 10(8):529. doi: 10.3390/diagnostics10080529
22. Gorgey AS, Khalil RE, Alrubaye M, Gill R, Rivers J, Goetz LL, et al. Testosterone and long pulse width stimulation (TLPs) for denervated muscles after spinal cord injury: a study protocol of randomised clinical trial. *BMJ Open.* (2022) 12(10):e064748. doi: 10.1136/bmjopen-2022-064748
23. Gosselin MC, Neufeld E, Moser H, Huber E, Farcito S, Gerber L, et al. Development of a new generation of high-resolution anatomical models for medical device evaluation: the virtual population 3.0. *Phys Med Biol.* (2014) 59(18):5287–303. doi: 10.1088/0031-9155/59/18/5287
24. Colella M, Liberti M, Apollonio F, Bonmassar G. A miniaturized ultra-focal magnetic stimulator and its preliminary application to the peripheral nervous system, 2020 Aug 6. In: Makarov SN, Noetscher GM, Nummenmaa A, editors. *Brain and Human Body Modeling 2020: Computational Human Models Presented at EMBC 2019 and the BRAIN Initiative® 2019 Meeting*. Cham: Springer (2021).
25. Colella M, Press DZ, Laher RM, McCliff CE, Rutkove SB, Cassarà AM, et al. A study of flex miniaturized coils for focal nerve magnetic stimulation. *Med Phys.* (2023) 50(3):1779–92. doi: 10.1002/mp.16148
26. Hasgall PA, Di Gennaro F, Baumgartner C, Neufeld E, Lloyd B, Gosselin MC, et al. “IT’IS database for thermal and electromagnetic parameters of biological tissues,” version 4.1. (2022). doi: 10.13099/VIP21000-04-1
27. Desai SS, Arbor TC, Varacallo M., Anatomy. Shoulder and upper limb, musculocutaneous nerve. In: *StatPearls*. Treasure Island, FL: StatPearls Publishing (2023). Available online at: <https://www.ncbi.nlm.nih.gov/books/NBK534199/> (updated September 4, 2023).
28. Bayot ML, Nasserreddin A, Varacallo M., Anatomy. Shoulder and upper limb, brachial plexus. In: *StatPearls*. Treasure Island, FL: StatPearls Publishing (2023). Available online at: <https://www.ncbi.nlm.nih.gov/books/NBK500016/> (updated July 24, 2023).
29. Kuhn A, Keller T, Micera S, Morari M. Array electrode design for transcutaneous electrical stimulation: a simulation study. *Med Eng Phys.* (2009) 31(8):945–51. doi: 10.1016/j.medengphy.2009.05.006
30. Ge Y, Ye S, Zhu K, Guo T, Su D, Zhang D, et al. Mediating different-diameter α nerve fibers using a biomimetic 3D TENS computational model. *J Neurosci Methods.* (2020) 346:108891. doi: 10.1016/j.jneumeth.2020.108891
31. Datta A, Bansal V, Diaz J, Patel J, Reato D, Bikson M. Gyri-precise head model of transcranial direct current stimulation: improved spatial focality using a ring electrode versus conventional rectangular pad. *Brain Stimul.* (2009) 2(4):201–7. doi: 10.1016/j.brs.2009.03.005
32. McIntyre CC, Richardson AG, Grill WM. Modeling the excitability of mammalian nerve fibers: influence of afterpotentials on the recovery cycle. *J Neurophysiol.* (2002) 87(2):995–1006. doi: 10.1152/jn.00353.2001
33. McIntyre CC, Grill WM. Extracellular stimulation of central neurons: influence of stimulus waveform and frequency on neuronal output. *J Neurophysiol.* (2002) 88(4):1592–604. doi: 10.1152/jn.2002.88.4.1592
34. Gaines JL, Finn KE, Slopeema JP, Heyboer LA, Polasek KH. A model of motor and sensory axon activation in the median nerve using surface electrical stimulation. *J Comput Neurosci.* (2018) 45(1):29–43. doi: 10.1007/s10827-018-0689-5
35. Pelot NA, Behrend CE, Grill WM. Modeling the response of small myelinated axons in a compound nerve to kilohertz frequency signals. *J Neural Eng.* (2017) 14(4):046022. doi: 10.1088/1741-2552/aa6a5f
36. Samoudi AM, Kampusch S, Tanghe E, Széles JC, Martens L, Kaniusas E, et al. Sensitivity analysis of a numerical model for percutaneous auricular vagus nerve stimulation. *Appl Sci.* (2019) 9(3):540. doi: 10.3390/app9030540
37. Roointan S, Tovbis D, Elder C, Yoo PB. Enhanced transcutaneous electrical nerve stimulation achieved by a localized virtual bipole: a computational study of human tibial nerve stimulation. *J Neural Eng.* (2020) 17(2):026041. doi: 10.1088/1741-2552/ab85d3
38. Anderson DN, Duffley G, Vorwerk J, Dorval AD, Butson CR. Anodic stimulation misunderstood: preferential activation of fiber orientations with anodic waveforms in deep brain stimulation. *J Neural Eng.* (2019) 16(1):016026. doi: 10.1088/1741-2552/aae590
39. Rattay F. Analysis of models for external stimulation of axons. *IEEE Trans Biomed Eng.* (1986) 33(10):974–7. doi: 10.1109/TBME.1986.325670
40. Duffley G, Anderson DN, Vorwerk J, Dorval AD, Butson CR. Evaluation of methodologies for computing the deep brain stimulation volume of tissue activated. *J Neural Eng.* (2019) 16(6):066024. doi: 10.1088/1741-2552/ab3c95
41. Butson CR, Cooper SE, Henderson JM, McIntyre CC. Patient-specific analysis of the volume of tissue activated during deep brain stimulation. *Neuroimage.* (2007) 34(2):661–70. doi: 10.1016/j.neuroimage.2006.09.034
42. Collu R, Earley EJ, Barbaro M, Ortiz-Catalan M. Non-rectangular neurostimulation waveforms elicit varied sensation and perceptible fields on the hand. *Sci Rep.* (2023) 13(1):1588. doi: 10.1038/s41598-023-28594-0
43. Thomas N, Osborn L, Moran C, Fifer M, Christie B. Wrist posture unpredictably affects perception of targeted transcutaneous electrical nerve stimulation with wrist-placed electrodes. *Front Neurosci.* (2024) 18:1490828. doi: 10.3389/fnins.2024.1490828
44. Blair HA. On the intensity-time relations for stimulation by electric currents. I. *J Gen Physiol.* (1932) 15(6):709–29. doi: 10.1085/jgp.15.6.709
45. Rattay F, Paredes LP, Leao RN. Strength-duration relationship for intra- versus extracellular stimulation with microelectrodes. *Neuroscience.* (2012) 214(5):1–13. doi: 10.1016/j.neuroscience.2012.04.004
46. Badran BW, Yu AB, Adair D, Mappin G, DeVries WH, Jenkins DD, et al. Laboratory administration of transcutaneous auricular vagus nerve stimulation (taVNS): technique, targeting, and considerations. *J Vis Exp.* (2019) (143):10.3791/58984. doi: 10.3791/58984
47. Niimi Y, Gomez-Tames J, Wasaka T, Hirata A. Selective stimulation of nociceptive small fibers during intraepidermal electrical stimulation: experiment and computational analysis. *Front Neurosci.* (2023) 16:1045942. doi: 10.3389/fnins.2022.1045942
48. Kuhn A, Keller T, Lawrence M, Morari M. A model for transcutaneous current stimulation: simulations and experiments. *Med Biol Eng Comput.* (2009) 47(3):279–89. doi: 10.1007/s11517-008-0422-z
49. Goffredo M, Schmid M, Conforto S, Bilotti F, Palma C, Vegni L, et al. A two-step model to optimise transcutaneous electrical stimulation of the human upper arm. *Compel Int J Comput Math Electr Electron Eng.* (2014) 33(4):1329–45. doi: 10.1108/COMP-04-2013-0118
50. Zhu K, Li L, Wei X, Sui X. A 3D computational model of transcutaneous electrical nerve stimulation for estimating α tactile nerve fiber excitability. *Front Neurosci.* (2017) 11:250. doi: 10.3389/fnins.2017.00250
51. Datta A, Zhou X, Su Y, Parra LC, Bikson M. Validation of finite element model of transcranial electrical stimulation using scalp potentials: implications for clinical dose. *J Neural Eng.* (2013) 10(3):036018. doi: 10.1088/1741-2560/10/3/036018
52. Huang Y, Liu AA, Lafon B, Friedman D, Dayan M, Wang X, et al. Measurements and models of electric fields in the in vivo human brain during transcranial electric stimulation. *Elife.* (2017) 6:e18834. doi: 10.7554/eLife.18834
53. Coates S, Thwaites B. The strength-duration curve and its importance in pacing efficiency: a study of 325 pacing leads in 229 patients. *Pacing Clin Electrophysiol.* (2000) 23(8):1273–7. doi: 10.1111/j.1540-8159.2000.tb00943.x
54. Deng ZD, Lisanby SH, Peterchev AV. Electric field depth-focality tradeoff in transcranial magnetic stimulation: simulation comparison of 50 coil designs. *Brain Stimul.* (2013) 6:1–13. doi: 10.1016/j.brs.2012.02.005
55. Haberbosch L, Datta A, Thomas C, Joos A, Köhn A, Rönnefarth M, et al. Safety aspects, tolerability and modeling of retinofugal alternating current stimulation. *Front Neurosci.* (2019) 13:783. doi: 10.3389/fnins.2019.00783
56. Truong DQ, Thomas C, Hampstead BM, Datta A. Comparison of transcranial focused ultrasound and transcranial pulse stimulation for neuromodulation: a computational study. *Neuromodulation.* (2022) 25(4):606–13. doi: 10.1016/j.neurom.2021.12.012
57. Guillen A, Abbott CC, Deng ZD, Huang Y, Pascoal-Faria P, Truong DQ, et al. Impact of modeled field of view in electroconvulsive therapy current flow simulations. *Front Psychiatry.* (2023) 14:1168672. doi: 10.3389/fpsyt.2023.1168672
58. Roth Y, Amir A, Levkovitz Y, Zangen A. Three-dimensional distribution of the electric field induced in the brain by transcranial magnetic stimulation using figure-8 and deep H-coils. *J Clin Neurophysiol.* (2007) 24:31–8. doi: 10.1097/WNP.0b013e31802fa393
59. Datta A, Dmochowski JP, Guleyupoglu B, Bikson M, Fregni F. Cranial electrotherapy stimulation and transcranial pulsed current stimulation: a computer based high-resolution modeling study. *Neuroimage.* (2013) 65:280–7. doi: 10.1016/j.neuroimage.2012.09.062
60. Cakmak YO, Nazim K, Thomas C, Datta A. Optimized electrode placements for non-invasive electrical stimulation of the olfactory bulb and olfactory mucosa. *Front Neurosci.* (2020) 14:581503. doi: 10.3389/fnins.2020.581503

61. Truong DQ, Guillen A, Nooristani M, Maheu M, Champoux F, Datta A. Impact of galvanic vestibular stimulation electrode current density on brain current flow patterns: does electrode size matter? *PLoS One*. (2023) 18(2):e0273883. doi: 10.1371/journal.pone.0273883

62. Truong DQ, Thomas C, Ira S, Valter Y, Clark TK, Datta A. Unpacking galvanic vestibular stimulation using simulations and relating current flow to reported motions: comparison across common and specialized electrode placements. *PLoS One*. (2024) 19(8):e0309007. doi: 10.1371/journal.pone.0309007

63. Jadidi AF, Jensen W, Zarei AA, Lontis ER, Atashzar SF. From pulse width modulated TENS to cortical modulation: based on EEG functional connectivity analysis. *Front Neurosci*. (2023) 17:1239068. doi: 10.3389/fnins.2023.1239068

64. Huang Y. Visualizing interferential stimulation of human brains. *Front Hum Neurosci*. (2023) 17:1239114. doi: 10.3389/fnhum.2023.1239114

65. Rampazo ÉP, Liebano RE. Analgesic effects of interferential current therapy: a narrative review. *Medicina (Kaunas)*. (2022) 58(1):141. doi: 10.3390/medicina58010141